Snapin-Mediated BACE1 Retrograde Transport Is Essential for its Degradation in Lysosomes and Regulation of APP Processing in Neurons

Xuan Ye and Qian Cai

Supplemental Information

I. Supplemental Figures and Figure Legends

Figure S1 (Cai)

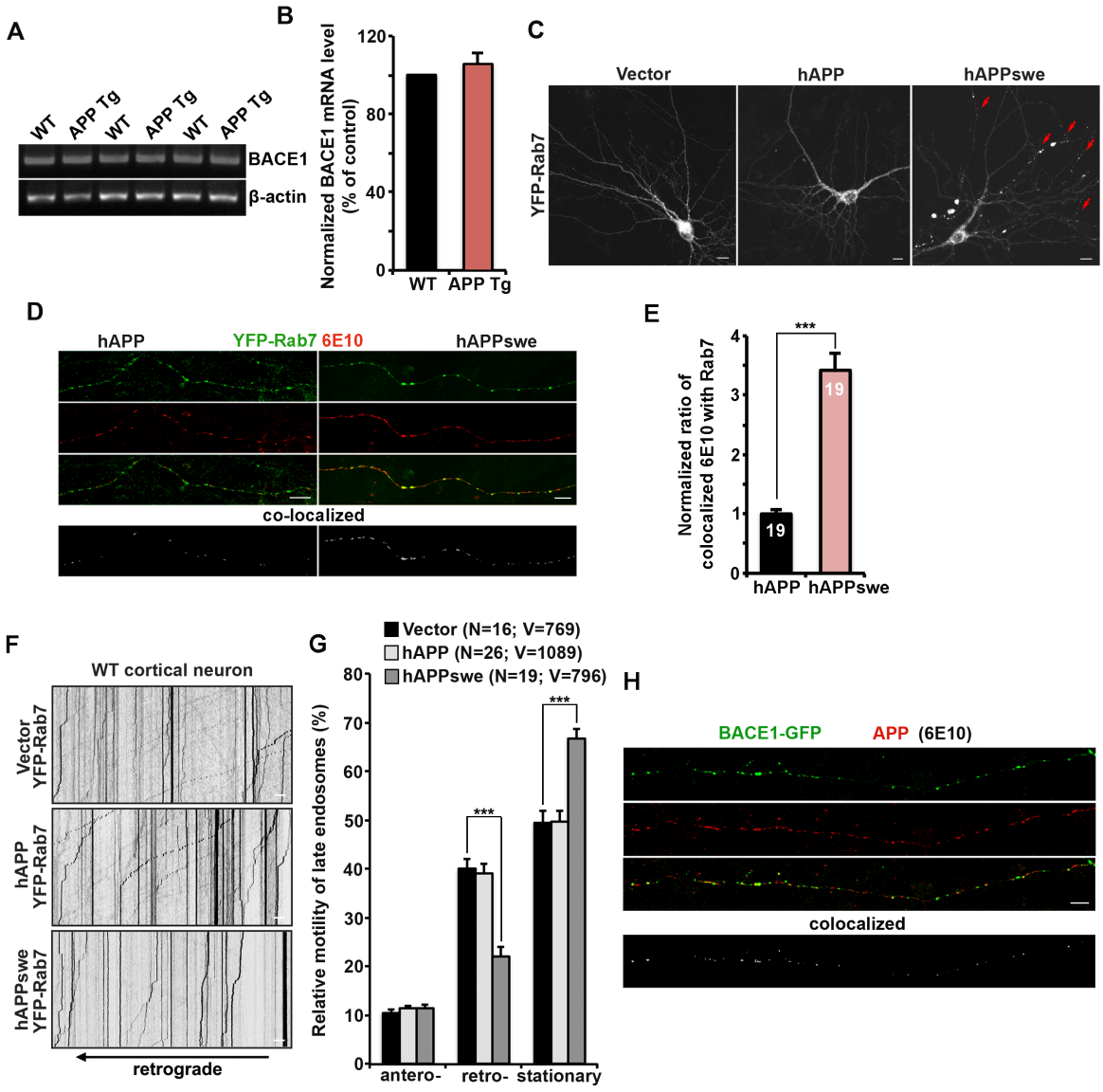

Figure S1. (Related to Figure 1) **Altered Late Endocytic Pathway in Cultured Cortical Neurons Expressing Mutant hAPPswe, but not Wild-Type hAPP, and Accumulation of BACE1 within APP-Enriched Vesicles along Axons**

(A, B) BACE1 mRNA levels (A) and quantitative analysis (B) showing no significant alteration in hAPP Tg mouse cortices at 11 to 15 months of age relative to WT littermates. Data were analyzed from 3 pairs of mice of each genotype, and expressed as Mean ± SEM. with Student *t* test.

(C) Representative images showing distribution pattern of late endosomes in cultured cortical neurons expressing vector, wild-type hAPP, or hAPPswe. Neurons were transfected at DIV6 and imaged at DIV10-11. Note that late endosomes in cortical neurons expressing hAPPswe appear to be clustered and accumulated at distal processes marked as red arrows, while they present as much smaller puncta and are more uniformly distributed in neurons expressing vector or hAPP.

(D, E) Representative axonal images (D) and quantitative analysis (E) showing increased late endosomal retention of APP and its cleaved products (C99 and Aβ) in neurons expressing hAPPswe. Neurons were transfected with YFP-Rab7 and hAPP or hAPPswe at DIV6, followed by co-immunostaining with anti-MAP2 and anti-6E10 antibodies at DIV10-11. MAP2-negative axons were selected for imaging.

(F, G) Representative kymographs (F) and quantitative analysis (G) of retrograde axonal transport of YFP-Rab7-labeled late endosomes in cortical neurons expressing vector, hAPP, or hAPPswe at DIV10-12. Vertical lines represent stationary organelles; lines to the left (positive slope) indicate retrograde transport. As an internal control, expressing hAPPswe has no effect on anterograde transport along the same axons. Data were quantified from a total number of axonal late endosomes (V) from a total number of neurons (N) in >3 experiments, as indicated in parentheses.

(H) Representative axonal images showing accumulation of BACE1 within APP- or its cleavage products (C99 or Aβ)-enriched vesicles along the axon of hAPP Tg neurons. Neurons were transfected with BACE1-GFP at DIV6 and co-immunostained with anti-MAP2 and anti-6E10 antibodies at DIV16. MAP2-negative axons were selected for imaging.

*** $p < 0.001$. Error bars: SEM. Student's *t* test. Scale bars in C, D, F, and H: 10 μm.

Figure S2 (Cai)

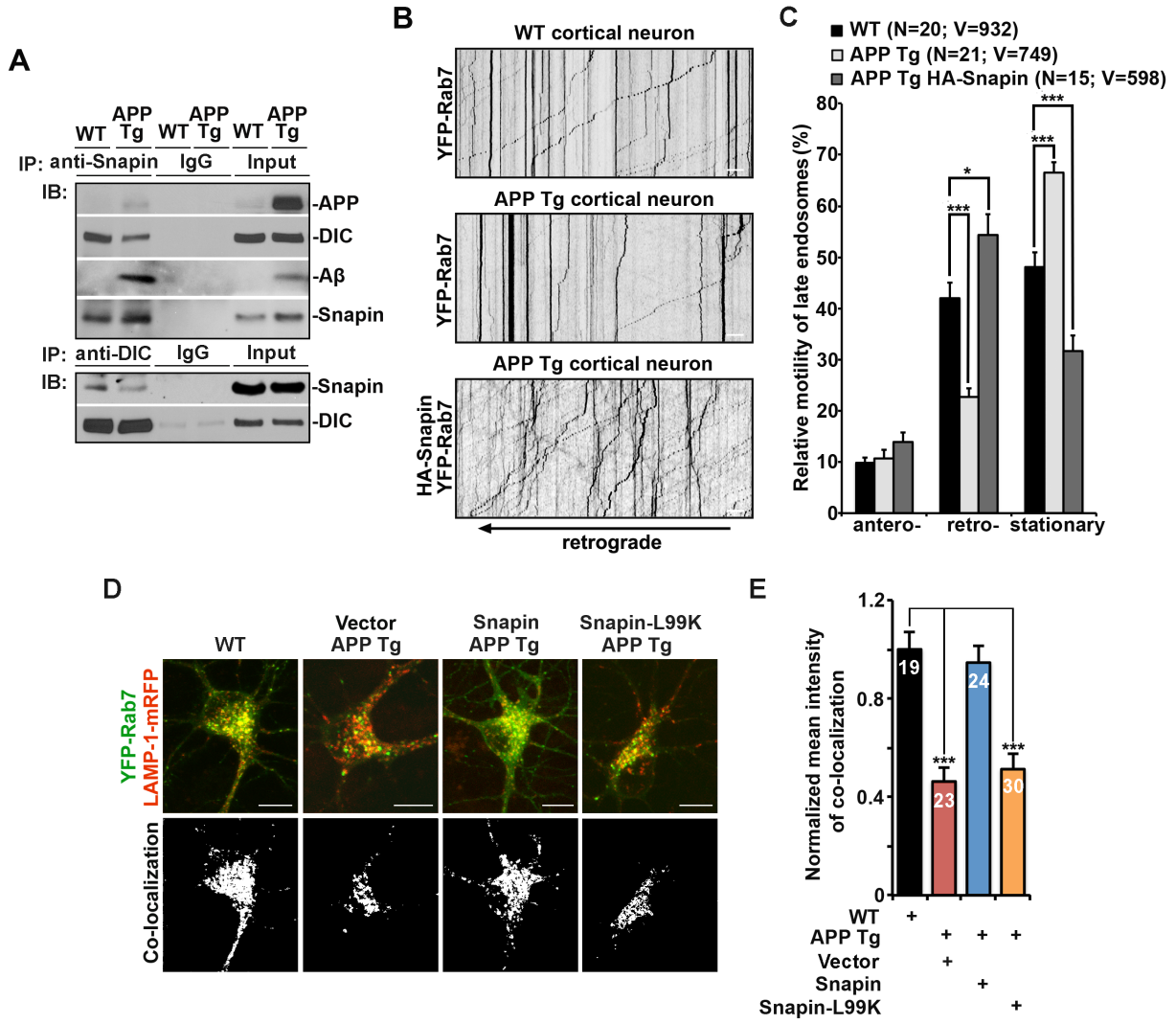

Figure S2. (Related to Figure 2) **Defective Late Endocytic Pathway due to Impaired Snapin-DIC Coupling in hAPP Mutant Neurons**

(A) Reciprocal co-immunoprecipitation assays showing reduced Snapin-DIC coupling in hAPP Tg mouse brains. Note that reduced amounts of the Snapin-DIC complex were reciprocally immunoprecipitated from hAPP Tg mouse brains with either an anti-Snapin or anti-DIC antibody, whereas Snapin associates with Aβ.

(B, C) Representative kymographs (B) and quantitative analysis (C) showing retrograde axonal transport of YFP-Rab7 in WT, hAPP mutant Tg neurons, and rescued hAPP mutant Tg neurons by expressing HA-Snapin at DIV9-12. Vertical lines represent stationary organelles; lines to the

left (positive slope) indicate retrograde transport. As an internal control, expressing Snapin has no effect on anterograde transport along the same axons. Data were quantified from a total number of axonal late endosomes (V) from a total number of neurons (N) in >3 experiments, as indicated in parentheses.

(D, E) Representative images (D) and quantitative analysis (E) of co-localized mean intensity showing reduced late endocytic trafficking in hAPP Tg neurons, which was rescued by expressing Snapin, but not Snapin-L99K mutant defective in DIC binding. Cortical neurons cultured from hAPP Tg mice were co-transfected with YFP-Rab7, LAMP-1-mRFP, and HA vector, HA-Snapin or HA-Snapin-L99K at DIV 6-7 and imaged at DIV 11-13. Normalized mean intensity for co-localization reflects relative late endocytic trafficking from Rab7-associated late endosomes to LAMP-1-labeled lysosomes in the soma. Data quantified from a total number of neurons were indicated on the top of bars from >3 experiments.

*** $p < 0.001$; ** $p < 0.01$; * $p < 0.05$. Error bars: SEM. Student's *t* test. Scale bar: 10 μm.

Figure S3 (Cai)

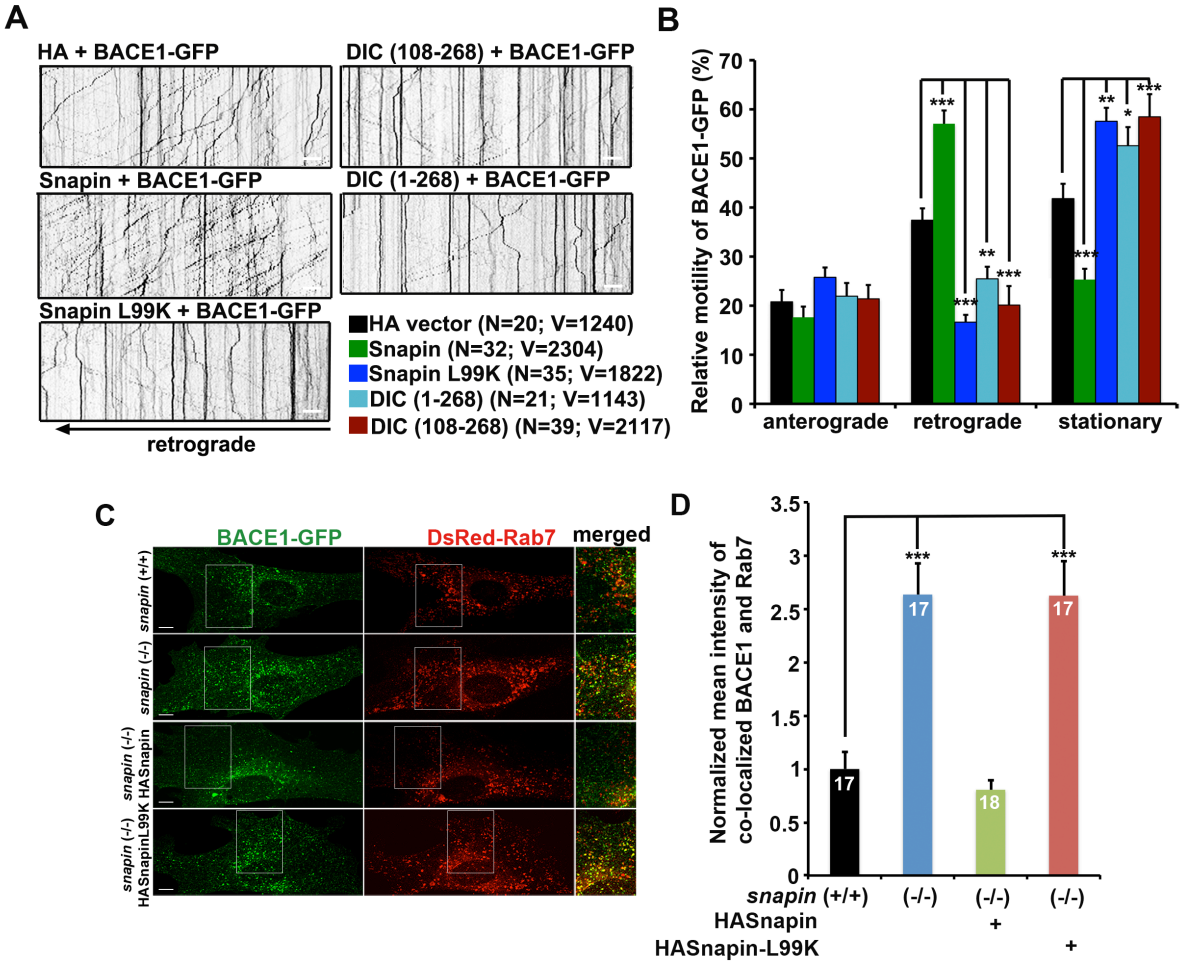

Figure S3. (Related to Figure 3) **Disruption of Snapin-DIC Coupling Impairs BACE1 Retrograde Transport and Accumulates BACE1 within Late Endosomes in *snapin*-Deficient MEFs**

(A, B) Disruption of Snapin-DIC coupling selectively inhibits BACE1 retrograde transport. Kymographs (C) and relative motility (D) of BACE1-containing vesicles were imaged during a 2-min period along axonal processes of WT neurons co-expressing BACE1-GFP with HA vector, or Snapin, or Snapin-L99K mutant, or DIC-truncated mutants (DIC108–268 or DIC 1–268). Cortical neurons were co-transfected at DIV6 and time-lapse images were taken at DIV9-10. Note that while elevated Snapin expression enhanced BACE1 retrograde transport, disrupting Snapin-DIC coupling by expressing dominant negative mutants of Snapin and DIC selectively impaired BACE1 retrograde transport. Relative motility was compared to control neurons transfected with HA vehicle vector control (black bars). Data were quantified from a total number

of axonal BACE1 cargos (V) from a total number of neurons (N) as indicated in parentheses (B) in >3 experiments.

(C, D) Representative images (C) and co-localized mean intensity analysis (D) showing the retention of BACE1 within late endosomes in *snapin*-deficient MEFs expressing BACE1-GFP and DsRed-Rab7. Images were taken from MEFs of *snapin* (+/+), *snapin* (-/-), or rescued cells by Snapin, or cells co-expressing DIC-binding defective Snapin-L99K mutant. Right panels (A) are close-up views of the boxed areas. Increased co-localization of the signal intensity reflects the accumulation of BACE1 within late endosomes, rather than the delivery to lysosomes for degradation. Note that expressing Snapin, but not Snapin-L99K, effectively reduces the retention of BACE1 within late endosomal compartments. Data were quantified from the total number of cells as indicated in the top of bars in 3 experiments.

Scale bars: 10 μm. Error bars: SEM. Student's *t* test. (***: $p < 0.001$; **: $p < 0.01$; *: $p < 0.05$).

Figure S4 (Cai)

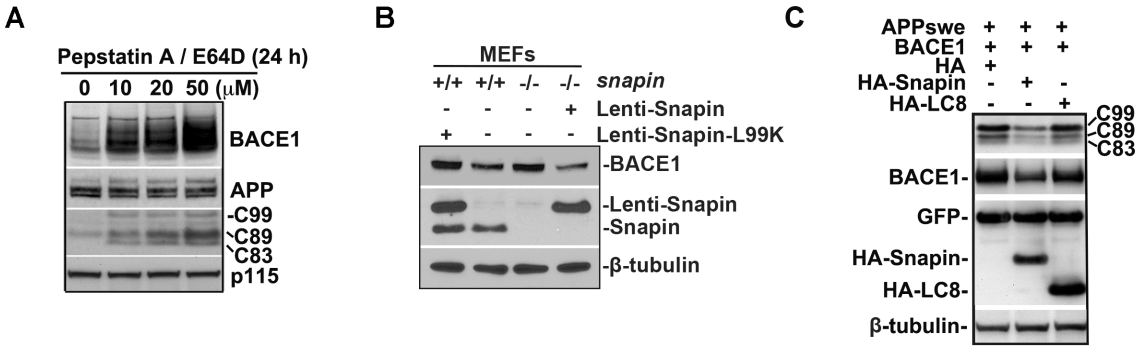

Figure S4. (Related to Figure 4) **Overexpressing Snapin Reduces BACE1 Levels in *snapin*-Deficient MEFs and COS7 cells**

(A) Lysosomal inhibition leads to increased levels of BACE1 and APP processing in neurons. Cultured WT hippocampal neurons were treated with increasing concentrations (10, 20 and 50 μM) of lysosomal inhibitors (Pepstatin A and E64D) for 24 hr. Cell lysates were solubilized and equal amounts of protein (20 μg) were loaded for sequential detection with antibodies on the same membrane after striping between applications of each antibody as indicated. Note that APP carboxyl-terminal fragments (CTFs) including APP-C99, APP-C89, and APP-C83, and BACE1 were detected in an increased level in cultured neurons treated with increasing doses of lysosomal inhibitors. This is a representative set of blots from three independent experiments.

(B) Reintroducing Snapin into *snapin*-deficient MEFs reduced endogenous BACE1, while overexpressing Snapin-L99K resulted in an elevated BACE1 level. WT and *snapin*-deficient MEFs were infected with Lenti-Snapin or Lenti-Snapin-L99K, respectively. Cell lysates were collected four days after infection, and equal amounts (20 μg) of lysates were sequentially detected on the same membrane with antibodies as indicated.

(C) Elevated Snapin expression inhibits APP processing by reducing BACE1. COS7 cells were co-transfected with APPswe, BACE1 and HA-Snapin, or HA controls (HA vector alone or HA-LC8). Cell lysates (20 μg) were processed for sequential detection with antibodies as indicated.

II. Supplemental Movie Captions

Movie S1. (Related to Figure 2E) **BACE1 Transport Along the Axonal Process of WT Cortical Neuron**

Cortical neurons were transfected with BACE1-GFP and HA vector at DIV6, followed by time-lapse imaging at DIV12. Movement to the left indicates retrograde transport. Note that BACE1 undergoes dynamic and bi-directional movement along axonal process. Time-lapse sequences were collected at 1-sec intervals during a 100-s observation.

Movie S2. (Related to Figure 2E) **BACE1 Transport Along the Axonal Process of hAPP Mutant Cortical Neuron**

Cortical neurons from hAPP mutant Tg (J20) mice were transfected with BACE1-GFP and HA vector at DIV6, followed by time-lapse imaging at DIV12. Movement to the left indicates retrograde transport. Note that BACE1 retrograde but not anterograde transport is selectively reduced. Time-lapse sequences were collected at 1-sec intervals during a 100-s observation.

Movie S3. (Related to Figure 2E) **BACE1 Transport Along the Axonal Process of hAPP Mutant Cortical Neuron overexpressing HA-Snapin**

Cortical neurons from hAPP mutant Tg (J20) mice were transfected with BACE1-GFP and HA-Snapin at DIV7, followed by time-lapse imaging at DIV12. Movement to the left indicates retrograde transport. Note that retrograde transport of BACE1 is rescued. Time-lapse sequences were collected at 1-sec intervals during a 100-s observation.

Movie S4. (Related to Figure 2E) **BACE1 Transport Along the Axonal Process of hAPP Mutant Cortical Neuron overexpressing HA-Snapin-L99K**

Cortical neurons from hAPP mutant Tg (J20) mice were transfected with BACE1-GFP and HA-Snapin-L99K at DIV6, followed by time-lapse imaging at DIV11. Movement to the left indicates retrograde transport. Note that reduced retrograde transport of BACE1 isn't reversed. Time-lapse sequences were collected at 1-sec intervals during a 100-s observation.

Movie S5. (Related to Figure 3A) **Axonal Transport of BACE1 in Homozygous *snapin Flox* Cortical Neuron**

Cortical neurons from homozygous *snapin flox* mice were transfected with BACE1-GFP at DIV6, followed by time-lapse imaging at DIV12. Movement to the left indicates retrograde transport.

Note that BACE1 undergoes dynamic and bi-directional movement along the axonal process. Time-lapse sequences were collected at 1-sec intervals during a 100-s observation.

Movie S6. (Related to Figure 3A) **BACE1 Transport Along the Axonal Process of *snapin*-Deficient Cortical Neuron**

Homozygous *snapin flox* cortical neurons were co-transfected with BACE1-GFP and Cre at DIV6, followed by time-lapse imaging at DIV13. Movement to the left indicates retrograde transport. Note that retrograde transport of BACE1 is selectively impaired. Time-lapse sequences were collected at 1-sec intervals during a 100-s observation.

Movie S7. (Related to Figure 3A) **BACE1 Transport Along the Axonal Process of Rescued *snapin*-Deficient Cortical Neuron**

Homozygous *snapin flox* cortical neurons were co-transfected with BACE1-GFP, Cre, and HA-Snapin at DIV6, followed by time-lapse imaging at DIV13. Movement to the left indicates retrograde transport. Note that introducing Snapin into the *snapin*-deficient neuron efficiently recruits stationary organelles into the retrograde motile pool. Time-lapse sequences were collected at 1-sec intervals during a 100-s observation.

III. Supplemental Results

Defects in Late Endocytic Pathway and Snapin-DIC Coupling in hAPP Tg Neurons

We conducted the reciprocal co-immunoprecipitation assays to isolate the Snapin-DIC complex from mouse brains using either an anti-Snapin or anti-DIC antibody. The Snapin-DIC coupling is markedly reduced in hAPP Tg mouse brains relative to those of WT controls. Snapin associated with Aβ, but not with mutant hAPP (Figure S2A). It was reported that Aβ is accumulated on the outer membranes of late endosomes especially in distal processes and synaptic compartments in neurons from APP Tg mice (Takahashi et al., 2002, 2004). We proposed that Snapin and Aβ form complexes on the surface of late endosomes, and this interaction might potentially interfere with the Snapin-DIC coupling, resulting in a reduced recruitment of dynein motor onto late endosomes. Gouras's group reported that Aβ42 monomers were mainly associated on the outer membranes of late endosomes, whereas Aβ42 oligomers were predominantly located inside of endosomal vesicles (Takahashi et al., 2002, 2004). In our future study, we will test whether Aβ monomers, but not its oligomers, are likely candidates for uncoupling Snapin-DIC interaction.

We next performed time-lapse imaging in live cortical neurons to monitor the relative motility of Rab7-labeled late endosomes along axons. In WT neurons, motile late endosomes underwent predominant retrograde transport toward the soma (of the total 52% motile, 9.9 ± 0.94% for anterograde and 42.0 ± 3.01% for retrograde) (Figure S2B and S2C). In contrast, hAPP mutant neurons showed reduced retrograde transport (22.77 ± 1.64%, $p < 0.001$), and thus relatively increased their ratio in the stationary phase, which is consistent with the results from the immunoisolation assay showing reduced loading of retrograde motor dynein to late endosomes and coimmunoprecipitation assays showing impaired Snapin-DIC coupling. Similar defects were observed in cortical neurons expressing hAPPswe, but not hAPP (Figure S1F and S1G). Moreover, elevated expression of Snapin in hAPP Tg neurons not only rescued the defective retrograde transport of late endosomes, but also further enhanced their retrograde transport ratio relative to WT neurons (anterograde: 13.92 ± 1.89%, retrograde: 54.41 ± 3.99%, $p < 0.001$) (Figure S2B and S2C). Thus, elevated Snapin expression recruits more late endosomes from the stationary pool into the retrograde motile pool, likely by increasing formation of the motor-adaptor (Snapin-DIC) complex specific for attaching late endosomes.

In neurons, internalized proteins and targeted materials are delivered by late endosomes from distal processes to the soma, where mature lysosomes are predominantly located, which is an essential step to bring these two organelles close enough to fuse with high efficiency for late endocytic trafficking and degradation (Overly and Hollenbeck, 1996; Cai et al., 2010; Lee et al., 2011). We previously showed that the defects in Snapin-DIC coupling in *snapin* mutant neurons sufficiently impair late endocytic trafficking (Cai et al, 2010). We further addressed whether impaired retrograde transport of late endosomes compromises the traffic to lysosomes in hAPP Tg neurons. We examined the co-localization between Rab7-labeled late endosomes and LAMP-1-marked lysosomes in soma. Compared with WT controls, the trafficking from late endosomes to lysosomes was dramatically reduced in hAPP Tg neurons (46.29 ± 5.43%, n = 23, $p < 0.001$). However, overexpression of Snapin, but not Snapin-L99K mutant defective in DIC binding, rescued the defects in late endocytic trafficking (Snapin: 94.6 ± 6.6%, n = 24; Snapin-L99K: 51.28 ± 6.25%, n = 30) (Figures S2D and S2E), which is attributable to an enhanced retrograde transport of late endosomes (Figure S2B and S2C). These results suggest that Snapin-DIC coupling is critical for proper late endocytic trafficking. Such a motor-adaptor coupling, however, is impaired in mutant hAPP neurons.

Disrupting Snapin-DIC Coupling Impairs BACE1 Retrograde Transport

To determine whether Snapin-mediated BACE transport occurs through its binding to dynein DIC, we expressed in WT neurons Snapin or its mutant Snapin-L99K, a DIC-binding defective mutant by replacing a single hydrophobic residue with lysine, or DIC truncated mutants containing the Snapin-binding domain, including DIC (108-268) and DIC (1-268). These transgenes have been previously confirmed as dominant-negative mutants by effectively disrupting the endogenous Snapin-DIC interaction and impairing retrograde transport of late endosomes in cortical neurons (Cai et al., 2010; Zhou et al., 2012). Consistently, expressing these transgenes in WT neurons selectively reduced BACE1 retrograde transport, thus recruiting more BACE vesicles into the stationary pool (Figure S3A and S3B). These phenotypes mimic what were found in *snapin*-deficient neurons (Figure 3A and 3B), suggesting that disruption of the Snapin-DIC coupling selectively impairs BACE1 retrograde transport.

Although BACE1 is enriched in neurons (Cai et al., 2001), it is also expressed in mouse fibroblasts and displays β-secretase activity (Wang et al., 2008). *Snapin* (-/-) mouse embryotic fibroblasts (MEFs) exhibited an accumulation of late endosomes due to its impaired membrane trafficking to lysosomes (Cai et al., 2010). By using these MEFs as our cell models, we further examined whether the defects in BACE1 transport sufficiently induce its retention within late endosomes. Both *snapin* (+/+) and *snapin* (-/-) MEFs were transfected with BACE1-GFP and DsRed-Rab7. Co-localized mean intensity of BACE1 and Rab7-labeled late endosomes was measured and normalized to those in *snapin* (+/+) MEFs (Figure S3C and S3D).

Expressing Snapin Enhances BACE1 Degradation

To address whether proper lysosomal function is crucial for BACE1 turnover, thus restricting APP processing, we treated hippocampal neurons with increasing doses of lysosomal inhibitors E64D and Pepstatin A. Sequential immunoblots from the same membranes demonstrated a robust increase of BACE1 levels associated with elevated CTFs following lysosomal inhibition in a dose-dependent manner, reflecting an enhanced APP amyloidogenic processing (Figure S4A). Moreover, elevated Snapin expression in *snapin*-deficient MEFs effectively rescued the phenotypes by reducing BACE1 level (Figure S4B), which is consistent with the results showing decreased retention of BACE1 within late endosomes (Figures S3C and S3D). Conversely, disrupting Snapin-DIC coupling via infection of WT MEFs with Lenti-Snapin-L99K mutant effectively increased BACE1 level (Figure S4B). Thus, these results consistently support our hypothesis that impaired retrograde transport contributes to the accumulation of BACE1 within

the altered late endocytic system.

IV. Supplemental Experimental Procedures

Mice

snapin flox mice and *snapin* (+/-) mice were provided by Z.H. Sheng (National Institute of Neurologic Disorders and Stroke, NIH, Bethesda, MD). CaMKIIα-tTA and tet-APPswe/ind mice were obtained from H. Cai (National Institute on Aging, NIH, Bethesda, MD). hAPP mice (C57BL/6J) from line J20 (Mucke et al., 2000) and Thy1-cre Tg mice (Campsall et al., 2002) were purchased from the Jackson Laboratory.

Materials

H. Cai kindly provided pAdTrack-GFP-CMV-hAPP and pAdTrack-GFP-CMV-hAPPswe and Polyclonal anti-BACE1 antibody. pBACE1-GFP was provided by W. Song. pDsRed-Rab7 and pLAMP-1-mRFP were from R.E. Pagano and D. Sabatini, respectively. P. Xie provided pBS185-Cre construct. The constructs encoding Snapin, Snapin-L99K, DIC (1–268), DIC (108–268), and YFP-Rab7 were prepared as previously described (Cai et al., 2010; Zhou et al., 2012). The purified polyclonal antibody against mouse N-terminal Snapin was described previously (Tian et al., 2005). Snapin constructs and polyclonal antibody were obtained from Z.H. Sheng. Sources of other antibodies and reagents are as follows: polyclonal anti-EEA1 antibody (Santa Cruz); monoclonal anti-DIC antibody, and polyclonal anti-APP c-terminal antibody (Millipore/CHEMICON); monoclonal anti-GFP (JL-8) antibody (Clontech); monoclonal anti-Rab7 and anti-β tubulin antibodies (Sigma); monoclonal anti-β Amyloid (6E10) and anti-HA antibodies (Covance); monoclonal anti-p115 antibody (BD Biosciences); Alexa fluor 546-, and 633-conjugated secondary antibodies (Invitrogen); Pepstatin A (Calbiochem); Leupeptin (Sigma). Monoclonal anti-LAMP1 and LAMP2 antibodies were developed by D Messner and JT August and were obtained from Developmental Studies Hybridoma Bank.

Transfection and Immunocytochemistry of Cultured Cortical Neurons

Cortices were dissected from E18-19 mouse embryos or P0 mouse pups as described (Goslin et al., 1998; Cai et al., 2010; Cai et al., 2012). Cortical neurons were dissociated by papain (Worthington) and plated at a density of 100,000 cells per cm^2 on polyornithine- and fibronectin-coated coverslips. Neurons were grown overnight in plating medium (5% FBS, insulin, glutamate, G5 and 1 x B27) supplemented with 100 x L-glutamine in Neurobasal medium

(Invitrogen). Starting at DIV 2, cultures were maintained in conditioned medium with half-feed changes of neuronal feed (1 x B27 in Neurobasal medium) every 3 days. Neurons were treated with lysosomal inhibitors for 24 hr, or transfected with various constructs at DIV6-8 using Lipofectamine 2000 (Invitrogen) followed by time-lapse imaging 3-10 days after transfection.

For immunostaining, cultured neurons were fixed with 4% formaldehyde (Polyscience, Inc.) and 4% sucrose (Sigma) in 1X phosphate-buffered saline (PBS) at room temperature (RT) for 20 min, or 100% ice-cold methanol at -20°C for 10 min, washed three times with PBS for 5 min each, and then incubated in 0.4% saponin, 5% normal goat serum (NGS), and 2% bovine serum albumin (BSA) in PBS for 1 hr. Fixed cultures were incubated with primary antibodies in PBS with 2% BSA and 0.4% saponin at 4°C overnight. Cells were washed four times with PBS at RT for 5 min each, incubated with secondary fluorescent antibodies at 1:400 dilution in PBS with 2% BSA and 0.4% saponin for 30 min, re-washed with PBS, and then mounted with Fluor-Gel anti-fade mounting medium (EMS) for imaging.

MEF and COS7 Cell Culture and Transfection

Mouse embryonic fibroblasts (MEFs) from *snapin* wild-type and mutant mice were obtained from Z.H. Sheng. Cells were incubated with high glucose DMEM containing sodium pyruvate, L-glutamine, supplemented with 10% FBS and penicillin-streptomycin (1×) (Invitrogen). Transient transfection of MEF cells or COS7 was performed using Lipofectamine 2000. 100 μl of Opti-MEM (Invitrogen) and 1-2 μl of Lipofectamine 2000 (Invitrogen) per chamber were pre-incubated at RT for 5 min and then mixed with 100 μl of Opti-MEM containing DNA constructs (2-3 μg per chamber) and incubated for 20 min at RT to allow complex formation. The entire mixture was added directly to cultured cells. Following transfection, cells were cultured for an additional 1-2 days before imaging or harvesting for biochemical analysis.

Tissue Preparation and Immunohistochemistry

Animals were anaesthetized with 2.5% avertin (0.5ml per mouse), and transcardially perfused with fixation buffer (4% paraformaldehyde in PBS, pH 7.4). Brains were dissected out and postfixed in fixation buffer overnight and then placed in 30% sucrose at 4°C. 10-μm-thick coronal sections were collected consecutively to the level of the hippocampus and used to study co-localization of various markers. After incubation with blocking buffer (2.5% goat serum, 0.15% Triton X-100, 1.5% BSA, 0.5% glycine in H_2O) at RT for 1 hr, the sections were incubated with primary antibodies at 4°C overnight, followed by incubating with secondary

fluorescence antibodies at 1:400 dilution at RT for 1 hr. After fluorescence immunolabeling, the sections were stained with DAPI, washed three times in PBS. The sections were then mounted with anti-fading medium (vector laboratories, H-5000) for imaging.

Image Acquisition and Quantification

Confocal images were obtained using an Olympus FV1000 oil immersion 60 × objective (1.3 numerical aperture) with sequential-acquisition setting. For fluorescent quantification, images were acquired using the same settings below saturation at a resolution of 1,024 × 1,024 pixels (8 bit). Eight to ten sections were taken from top-to-bottom of the specimen and brightest point projections were made. Co-localization and morphometric measurements were performed using NIH ImageJ. Measured data were imported into Excel software for analysis. The thresholds in all images were set to similar levels. Co-localized fluorescence intensity from the *snapin*-deficient MEFs was finally normalized to that from control WT cells. Data were obtained from at least three independent experiments and the number of cells used for quantification is indicated in the figures. All statistical analyses were performed using the Student's *t*-test and are presented as mean ± SEM.

For live cell imaging, cells were transferred to Tyrode's solution containing 10 mM Hepes, 10 mM glucose, 1.2 mM $CaCl_2$, 1.2 mM $MgCl_2$, 3 mM KCl and 145 mM NaCl, pH 7.4. Temperature was maintained at 37°C with an air stream incubator. Cells were visualized with a 60× oil immersion lens (1.3 numerical aperture) on a Olympus FV1000 confocal microscope, using 488 nm excitation for GFP or YFP and 543 nm for DsRed or mRFP. Time-lapse sequences of 1,024×1,024 pixels (8 bit) were collected at 1-2 sec intervals with 1% intensity of the argon laser to minimize laser-induced bleaching and damage to cells, and maximum pinhole opening. Time-lapse images were captured by a total of 100 frames. All recordings started 6 min after the coverslip was placed in the chamber. The stacks of representative images were imported into NIH ImageJ. A membranous organelle was considered stopped if it remained stationary for the entire recording period; a motile one was counted only if the displacement was at least 5 μm.

For analyzing the motility of BACE1 vesicles or Rab7 in live neurons, we selected axons for time-lapse imaging and measuring motility because axons, but not dendrites, have a uniform microtubule organization and polarity. Axonal processes were selected as we previously reported (Kang et al., 2008; Cai et al., 2010, 2012). Briefly, axons in live images were

distinguished from dendrites based on known morphological characteristics: greater length, thin and uniform diameter, and sparse branching (Banker and Cowan, 1979). Only those that appeared to be single axons and separate from other processes in the field were chosen for recording axonal BACE1 or Rab7 transport. Regions where crossing or fasciculation occurred were excluded from analysis.

Kymographs were used to trace axonal anterograde or retrograde movement of membranous organelles and to count stationary ones as described previously (Miller and Sheetz, 2004; Kang et al., 2008) with extra plug-ins for ImageJ (NIH). Briefly, we used the "Straighten" plugin to straighten curved axons and the "Grouped ZProjector" to z-axially project re-sliced time-lapse images. The height of the kymographs represents recording time (100 sec unless otherwise noted), while the width represents the length (μm) of the axon imaged. Counts were averaged from 100 frames for each time-lapse image to ensure accuracy of stationary and motile events. Measurements are presented as mean ± SEM. Statistical analyses were performed using unpaired Student's *t*-tests.

Fluorescent signal co-localization was determined by automatically quantifying pixels containing both fluorescent signals and scored by ImageJ based on the fluorescence intensity profile and expressed as co-localized mean intensity positive for both BACE1-GFP and LAMP-1-mRFP or DsRed-Rab7. Pixel values of co-localization from APP Tg cortical neurons or *snapin*-deficient neurons or MEFs were finally normalized to those from control cells. Data were obtained from at least three independent experiments and the number of cells used for quantification is indicated in the figures.

Immunoisolation of Late Endocytic Organelles

Brain tissues from WT or APP Tg mice were homogenized in the buffer (10 mM HEPES [pH 7.4], 1 mM EDTA, 0.25 M sucrose, and protease inhibitors) and centrifuged at 800 × g for 10 min, and the supernatant was collected. The pellet was re-suspended in the homogenization buffer using a glass rod with 3 to 4 gentle strokes of the pestle of the 30-ml Dounce Homogenizer and re-centrifuged at 800 × g for 10 min. The combined first and second supernatants were centrifuged at 3,500 × g for 10 min and then collected for high-speed centrifugation at 20,000 × g for 10 min. The pellet was re-suspended in the homogenization buffer using a glass rod with 3 to 4 gentle strokes of the pestle of the 30-ml Dounce Homogenizer and re-centrifuged at 20,000 × g for 10 min. The pellet was then re-suspended in

the homogenization buffer and subjected to immuno-isolation with tosylated linker-coated superparamagnetic beads (Dynabeads M-450 Subcellular; Invitrogen) as previously described (Cai et al., 2010; Zhou et al., 2012). For all subsequent steps, beads were collected with a magnetic device (MPC; Invitrogen). After washing once for 5 min in PBS (pH 7.4) with 0.1% BSA at 4°C, the linker-coated beads (1.4 mg) were incubated with 1 μg anti-Rab7 mAb, or control mouse IgG overnight at 4°C on a rotator. After incubation, the beads were washed four times (5 min each) in PBS [pH 7.4] with 0.1% BSA at 4°C, and then re-suspended in an incubation buffer containing PBS [pH 7.4], 2 mM EDTA, 5% fetal bovine serum. Approximately 200 μg of light membrane fraction from WT or APP Tg mouse brains were mixed with incubation buffer containing beads (final reaction volume 1 ml) and incubated for 4 hr at 4°C on a rotator. After incubation, the beads were collected with a magnetic device and washed five times with the incubation buffer and three times with PBS for 10 min each and then resolved by 4-12% Bis-Tris PAGE for sequential Western blots on the same membranes after stripping between each application of the antibody. For semi-quantitative analysis, protein bands detected by ECL were scanned into Adobe Photoshop CS6, and analyzed using NIH ImageJ.

Immunoprecipitation

An equal amount (~750 μg) of brain homogenates from WT or hAPP Tg mouse cortices were incubated with anti-Snapin or anti-DIC antibody in 200 μl of TBS with 0.1% Triton X-100 and protease inhibitors, and incubated on a rotator at 4°C for overnight. 2.5 mg Protein A-Sepharose CL-4B resin (GE Healthcare) were added to each sample, and the incubation continued for an additional 3 hr followed by three washes with TBS/0.1% Triton X-100. Immobilized protein complexes were processed for SDS-PAGE and immunoblotting on the same membranes after stripping between each application of the antibody.

Measurement of Mouse Aβ Levels

Mouse Aβ40 ELISA kit (catalog no. KMB3481, Invitrogen) was used to detect Aβ40 levels in cortex or hippocampus in control and *snapin*$^{-/-}$ mouse brains. In brief, the cerebral cortex or hippocampus for ELISA was homogenized in 8× mass of cold guanidine buffer (5M guanidine HCl / 50mM Tris HCl, pH 8.0). The homogenates were then diluted (at 1:10) with cold reaction buffer BSAT-DPBS (Dulbecco's phosphate buffered saline with 5% BSA and 0.03% Tween-20 plus 1× protease inhibitor cocktail). The supernatants were collected after centrifugation (16,000g for 20 min at 4°C), and subjected to ELISA analysis using the kit according to the manufacturer's instructions.

Lentiviral Infection

Lenti-Snapin vector (provided by Z.H. Sheng) was generated by using the pLenti7.3/V5-TOPO TA Cloning Kit (Invitrogen). Lentiviral vectors were produced and purified according to the manual of ViralPower HiPerform Lentiviral Expression System (Invitrogen). Briefly, the recombinant lentivirus was prepared by cotransfecting the transfer vector with mixed three helper plasmids into 293LTV cells (obtained from P. Xie), and purified by ultracentrifugation. After 6-7 days in culture, cortical neurons from APP Tg P0 pups were infected with Lenti-Snapin. Five days later, cortical neuron lysates were harvested for biochemical analysis. MEF cells were transduced twice before harvesting lysates.

Semi-quantitative RT-PCR Analysis

Total RNA was isolated from mouse brain tissues using Trizol reagent (Invitrogen) according to the manufacturer's instructions. AMV reverse transcriptase XL (Takara) was used to synthesize the first-strand of cDNA from an equal amount of the RNA sample (0.5 μg). The newly synthesized cDNA templates were further amplified by *Takara Ex Taq* HS polymerase (Takara). Twenty-five to thirty-five cycles of PCR were used to cover the linear range of the PCR amplification. The BACE1 gene-specific primers 5′-CCACAGACGCTCAACATCCTG-3′ and 5′-CAATGATCATGCTCCCTCCCA-3′ were used to amplify a 452-bp fragment of the BACE1 gene coding region. The primers 5′-CCGTGAAAAGATGACCCAGAT-3′ and 5′-CCATACCCAAGAAGGAAGGCT-3′ were used to amplify a 463-bp fragment of the β-actin gene for internal controls. The samples were further analyzed on a 1.5% agarose gel. NIH ImageJ software was used to analyze the data.

V. Supplemental Discussion

While recent studies showed dynamic transport of BACE1 along neurites in cultured hippocampal neurons, this traffic route was also proposed to be responsible for the trafficking of BACE1 to the TGN mediated by VPS35, the core element of the retromer complex (Wen et al., 2011; Wang et al., 2012). However, six lines of evidence consistently support that Snapin and VPS35 play different roles in sorting/trafficking of BACE1. First, Snapin links the dynein motors to late endosomes, not the TGN. Second, Snapin-mediated BACE1 transport is selective for lysosomal targeting. Third, the defects in endosome-TGN trafficking were not observed in *snapin*-deficient neurons (Cai et al., 2010). Fourth, *snapin* deficiency results in BACE1

selectively accumulated within late endocytic compartments and reduced targeting to lysosomes. Fifth, elevated Snapin expression facilitates BACE1 turnover via enhanced retrograde transport and lysosomal delivery. In addition, VPS35 is enriched in TGN and early endosomes, and exhibits short-range movement in hippocampal neurons (Bhalla et al., 2012), while Snapin mediates long-range retrograde transport of BACE1-assocaited late endosomes.

In addition to BACE1 trafficking defects, Snapin-dynein coupling deficiency has a more general impact on the degradation and turnover of other endocytic components including EGFR (Cai et al., 2010). Consistently, a previous study that showed a delayed degradation of EGFR in hAPP mutant neurons (Almeida et al., 2006) further supports our notion. Our study revealed that APP presents within late endocytic organelles, and accumulates together with BACE1 in hAPP Tg neurons and mouse brains (Figures 1D, S1H, and 2B), indicating that late endocytic trafficking may play a critical role for the delivery of APP to lysosomes for degradation. Given that amyloidogenic processing appears to preferentially occur in the endosomal route, the intracellular trafficking of APP is thus critical for the regulation of Aβ generation.

VI. Supplemental References

Almeida, C,G, Takahashi, R.H, and Gouras, G.K. (2006). Beta-amyloid accumulation impairs multivesicular body sorting by inhibiting the ubiquitin-proteasome system. J Neurosci *26*, 4277-4288.

Banker, G.A., and Cowan, W.M. (1979). Further observations on hippocampal neurons in dispersed cell culture. J Comp Neurol *187*, 469-493.

Bhalla, A., Vetanovetz, C.P., Morel, E., Chamoun, Z., Di Paolo, G., and Small, S.A. (2012). The location and trafficking routes of the neuronal retromer and its role in amyloid precursor protein transport. Neurobiol Dis *47*, 126-134.

Campsall, K.D., Mazerolle, C.J., De Repentingy, Y., Kothary, R., and Wallace, V.A. (2002). Characterization of transgene expression and Cre recombinase activity in a panel of Thy-1 promoter-Cre transgenic mice. Dev Dyn *224*, 135-143.

Goslin, K., Asmussen, H., and Banker, G. (1998). Rat hippocampal neurons in low density. Culturing Nerve Cells. 2nd ed. G. Banker and K. Goslin, editors. M.I.T. Press, Cambridge, MA. 339-370.

Kang, J.S., Tian, J.H., Pan, P.Y., Zald, P., Li, C., Deng, C., and Sheng, Z.H. (2008). Docking of axonal mitochondria by syntaphilin controls their mobility and affects short-term facilitation. Cell *132*, 137-148.

Miller, K.E., and Sheetz, M.P. (2004). Axonal mitochondrial transport and potential are correlated. J Cell Sci *117*, 2791-2804.

Overly, C.C., and Hollenbeck, P.J. (1996). Dynamic organization of endocytic pathways in axons of cultured sympathetic neurons. J Neurosci *16*, 6056-6064.

Tian, J.H., Wu, Z.X., Unzicker, M., Lu, L., Cai, Q., Li, C., Schirra, C., Matti, U., Stevens, D., Deng, C.*, et al.* (2005). The role of Snapin in neurosecretion: snapin knock-out mice exhibit impaired calcium-dependent exocytosis of large dense-core vesicles in chromaffin cells. J Neurosci *25*, 10546-10555.

Wang, L., Shim, H., Xie, C., and Cai, H. (2008). Activation of protein kinase C modulates BACE1-mediated beta-secretase activity. Neurobiol Aging *29*, 357-367.

Wen, L., Tang, F.L., Hong, Y., Luo, S.W., Wang, C.L., He, W., Shen, C., Jung, J.U., Xiong, F., Lee, D.H.*, et al.* (2011). VPS35 haploinsufficiency increases Alzheimer's disease neuropathology. J Cell Biol *195*, 765-779.